Article type : Original Research Article

Terrestrial Microbialites Provide Constraints on the Mesoproterozoic Atmosphere

Hren, M.T.[1,2*], Sheldon, N.D.[3]

[1]Center for Integrative Geosciences, University of Connecticut, 354 Mansfield Dr., Storrs, CT 06269

[2]Department of Chemistry, University of Connecticut, 55 N. Eagleville Rd., Storrs, CT 06269

[3]Department of Earth & Environmental Sciences, University of Michigan, 1100 N. University Ave., Ann Arbor, MI 48109

*Corresponding Author. hren@uconn.edu

ABSTRACT

Palaeoclimate data indicate that Earth surface temperatures have remained largely temperate for the past 3.5 Byr despite significantly lower solar luminosity over this time relative to the present-day. There is evidence for episodic early and late Proterozoic glaciation, but little evidence of glaciation in the intervening billion years. A prolonged equable Mesoproterozoic Earth requires elevated greenhouse gas concentrations. Two end-member scenarios have been proposed for maintaining global warmth. These include extremely high pCO_2 or more modest pCO_2 with higher methane concentrations. This paper reports on the $\delta^{13}C$ of organic matter in 1.1

Ga stromatolites from the Copper Harbor Conglomerate (CHC) of the Mesoproterozoic Midcontinent Rift (N. America) and $\delta^{18}O$ and Δ_{47} temperatures of inorganic stromatolite carbonate to constrain formation and burial conditions and the magnitude of ancient carbon isotope discrimination. CHC sediments have never been heated above ~125–155°C, providing a novel geochemical archive of the ancient environment. Stromatolite Δ_{47} data record moderate alteration and therefore the occluded organic matter was unlikely to have experienced significant thermal alteration after deposition. The $\delta^{13}C$ values of ancient mat organic matter and inorganic carbonate show isotope discrimination (ε_p) values ~15.5 to 18.5‰, similar to modern microbial mats formed in equilibrium with low concentrations of dissolved inorganic carbon. In combination, these data are consistent with a temperate climate Mesoproterozoic biosphere supported by relatively modest pCO_2. This result agrees with Atmosphere-Ocean Global Circulation Model reconstructions for Mesoproterozoic climate using 5–10 times present atmospheric levels pCO_2 and pCH_4 of >28 ppmv. However, given marine modelling constraints of CH_4 production that suggest pCH_4 was below 10 ppm, this creates a methane paradox. Either an additional source of CH_4 (e.g. from terrestrial ecosystems) or another greenhouse gas, such as N_2O, would have been necessary to maintain equable conditions in the Mesoproterozoic.

Keywords (Clumped Isotopes, Mesoproterozoic, Mid-Continent Rift System, pCO_2, Stromatolites)

1. Introduction

Constraints on Earth surface temperature and atmospheric composition provide critical insight regarding the evolution of the biosphere (Kasting, 1993). The Mesoproterozoic has long been considered to be part of the "boring billion" years between the Palaeoproterozoic Huronian and Neoproterozoic "snowball Earth" events, when there was comparatively little change in Earth surface, greenhouse gas, or oceanic conditions (Lyons et al., 2014; Planavsky et al., 2014; Shields and Veizer, 2002) accompanied by relatively steady atmospheric pO_2. More recently though, new data indicate complex patterns of oceanic oxygenation and euxinia through time (Planavsky et al., 2014, 2018) and suggest that by the mid-Proterozoic, atmospheric pCO_2 likely dropped to less than one quarter of the Palaeoproterozoic levels (Kaufman and Xiao, 2003;

Sheldon, 2006; 2013). For example, Kanzaki and Murakami (2015) estimate 23–210 times present atmospheric levels (x PAL) at 1.85 Ga based on palaeosol geochemistry, but a number of studies have estimated the pCO_2 of the Mesoproterozoic (Bartley and Kah, 2004; Kah and Riding, 2007; Kaufman and Xiao, 2003; Mitchell and Sheldon, 2010) and report widely varying, but generally much lower estimates. For example, Kaufman and Xiao (2003) give an estimate of 10–200x PAL pCO_2 at 1.4 Ga based on the carbon isotopic composition of large microfossils, Kah and Riding (2007) give an estimate of ≤10x PAL at 1.2 Ga based on microbialite sheath calcification, and a number of palaeosols from the Midcontinental Rift (Mitchell and Sheldon, 2010; Sheldon, 2013) have consistently indicated 4-6x PAL at 1.1 Ga. A fundamental question is whether or not pCO_2 of this range could maintain temperate, non-glacial conditions without an additional greenhouse gas present. Given that a variety of proxies are consistent with low atmospheric pO_2 in the Mesoproterozoic (reviewed in Planavsky et al., 2018), CH_4 would likely have been stable in the atmosphere, and given that it has a warming potential about 25 times that of CO_2, it has often been proposed as a candidate Proterozoic greenhouse gas (Sheldon, 2013).

However, recent work suggests that anaerobic oxidation of CH_4 coupled with SO_4^{2-} reduction may have limited the flux of CH_4 from marine systems and potentially limited the buildup of CH_4 in the Proterozoic atmosphere (Olson et al., 2016). If this is correct, higher pCO_2 or elevated amounts of some other additional greenhouse gas would be needed to maintain temperate conditions. Constraints from the rock record (see Supplemental Table DR1 from Fiorella and Sheldon (2017)) indicate no evidence for glaciation at this time, except at one locality, to at least 60° N and S. New Atmospheric-Ocean Global Circulation Model (AOGCM) results show that modest (5–10x PAL) concentrations of CO_2 could maintain a largely ice-free globe with a range of pCH_4 from 28–280 ppmv (Fiorella and Sheldon, 2017), although a completely ice-free globe is only possible at the highest total greenhouse gas loads. Thus, Zhao et al. (2017) have described the late Mesoproterozoic as a potential methane paradox.

Morphological evidence for microbialite abundance and diversity indicate maxima for both during the Mesoproterozoic (Noffke and Awramik, 2013). Some argue that this is due to the evolution of new carbonate concentration mechanisms in the sheaths of cyanobacteria (Riding, 2011) that could have evolved in response to changing atmospheric conditions. Continental environments might have been even more chemically favourable for habitation than marine environments (Parnell et al., 2015) at this time. A range of evidence supports episodic glaciation

during the early and late Proterozoic (Kaufman et al., 1997; Kendall et al., 2004; Kennedy et al., 1998; Walter et al., 2000), but there is little or no evidence of prolonged, widespread glaciation during the Mesoproterozoic (Supplemental Table 1 of Fiorella and Sheldon (2017)). Thus, the inferred increase in microbialite abundance and diversity occurs during a time of clement conditions and of broad potential ecological niches including marine (Kah et al., 1999), transitional (Beghin et al., 2017), and terrestrial environments (Wellman and Strother, 2015). In total, biological and sedimentological evidence suggest a robust biosphere with globally temperate, ice-free conditions during this prolonged interval. If the Mesoproterozoic was a period of general and prolonged warmth, was high CO_2 responsible for the lack of glaciation?

This study presents new clumped and organic isotopic analyses of low thermal maturity stromatolites from Horseshoe Harbor, Michigan, within the Copper Harbor Conglomerate of the Mesoproterozoic-aged Mid-Continent Rift. Recent work demonstrates that these mats and associated geologic formations are minimally altered and have experienced limited heating in the 1.1 Byr since deposition (Nishioka, 1988; Gallagher et al., 2017). Clumped isotope temperatures provide some constraint on maximum formation temperatures and the potential for burial alteration of the organic isotopes, making it possible to use paired records of organic and inorganic carbon isotopes as a semi-quantitative indicator of atmospheric gas concentration.

2. Geologic Setting

2.1 Mid Continent Rift System

The Mid Continent Rift System (MCR; Figure 1) represents a widespread, failed continental rifting event that is characterized by large-scale emplacement of flood basalts that occurred in multiple pulses of volcanism ~1.1 Ga (Cumming et al., 2013; Davis and Paces, 1990; Hutchinson et al., 1990; Ohr, 1993). Rifting and extension is associated with widespread sedimentary deposition during early rift subsidence and records a classic continental rift sequence of alluvial fan sediments that transition to lacustrine and fluvial systems (Elmore et al., 1989; Mitchell and Sheldon, 2009; 2016). These igneous and clastic sedimentary units are collectively referred to as the Keweenaw Supergroup (Morey and Ojakangas, 1982). On the

eastern side of the rift, this includes lower volcanic strata through sedimentary strata of the Oronto Group, terminating in overlying sandstone units.

In Michigan (USA), the clastic sediments of the Oronto Group consist of the Copper Harbor Conglomerate (CHC), Nonesuch and Freda formations, corresponding to the alluvial fan, lacustrine, and fluvial deposits that span the rift interval (Elmore et al. 1984).The main stage of the MCR (Figure 1) occurred over a period of less than 50 Myr (Cannon and Hinze, 1992) and rifting was soon followed by regional compression that drove reactivation and reversal of rift bounding faults (Stein et al., 2015) associated with uplift of rift sediments. The rapid process of rifting and resultant regional compression means that rift sediments (Figure 1) were shallowly buried and minimally heated in some parts of the rift (<125°C; Mauk and Hieshima, 1992). This is due to the absence of large regional tectonic deformation in the mid-continent and the relatively short duration of rifting (Pratt et al., 1991; Price et al., 1996). The MCR experienced prehnite-pumpellyite grade metamorphism in places close to the basin-bounding faults, but thermal history models of available temperature constraints from the Nonesuch and CHC formations within the MCR indicate both low peak burial temperatures and a relatively short duration of burial before unroofing (Gallagher et al., 2017). Fluid inclusion studies of CHC microbial mats show that isolated inclusions homogenize at temperatures as low as 53 to 88°C (Nishioka et al., 1984). These low temperatures contrast with fluid inclusion data from carbonates directly associated with copper mineralization that show homogenization temperatures up to 119°C (Livnat, 1983). Thus, Nonesuch and CHC localities that are away from basin bounding faults typically experienced relatively mild thermal alteration to temperatures well below experimental constraints for abiotic Fischer-Tropsch synthesis of organic compounds (i.e. 250°C, high pressure; McCollom and Seewald, 2006).

2.2 Evidence for Life and Temperate Conditions in the MCR

The MCR extends from Kansas to Ontario and preserves a variety of textural evidence for life (Noffke 2009; Noffke and Awramik 2013; Sheldon 2012; Wilmeth et al. 2014) that support interpretations of a widely distributed terrestrial biosphere at 1.1 Ga. (Figures 2 and 3). This includes a number of fossil-bearing lake (Wellman and Strother, 2015), pond (Elmore, 1983), and floodplain deposits (Sheldon, 2012) that preserve an array of acritarchs, stromatolites,

and microbially-induced sedimentary structures. The stromatolites are found primarily in the CHC at two localities, and are interpreted to have formed in the distal parts of an alluvial fan where braided streams emptied into a large lake system associated with the Nonesuch Formation shale and mudstone deposition (Figure 2). These sediments display similarities to modern playa mudflats (Nishioka et al., 1984) and preserve evidence of desiccation features in both mudflat/sandflat and braidplain facies (Fedorchuk et al., 2016). Stromatolitic structures show alternation between detrital and carbonate laminae (Figures 2 and 3), with radial calcite overgrowths in some areas of the laminae (Elmore, 1983), and both abiogenic and biogenic forms have been identified (Fedorchuk et al., 2016). Both within the CHC (Wilmeth et al., 2014) and elsewhere within the MCR (Sheldon, 2012), other domal microbialite features have been noted, including some with preserved organic matter, suggesting a wide array of potential microbial communities and inhabited environmental niches at this time. Previous workers have demonstrated the potential for using the clumped isotope composition of similar microbialites in the geologic record to reconstruct environmental conditions at the time of their formation in lake and lake margin deposits. These studies show that modern and ancient microbial carbonates reasonably record the temperature of past surface water conditions, though they may be biased by variations in timing of precipitation or formation depths (Frantz et al., 2014; Petryshyn et al., 2015).

3. Methods

Stromatolites within CHC sediments at Horseshoe Harbor contain both calcitic laminae preserved in fine growth layers and sparite present in in-filled voids and larger, secondary fractures (Elmore, 1983, 1984). Samples were collected from the CHC in 2011, cut using a solvent-cleaned, water-cooled rock saw and polished using a diamond grit polish. Thin sections were analyzed to identify areas with no or minimal alteration of primary laminae. Samples of pristine carbonate laminae and secondary sparite were drilled at low speed using a Micromill to evaluate potential spatial variability in isotopic data. Drilled areas were specifically chosen to minimize any potential contamination with visible secondary carbonate. This had the effect of limiting the sample size available for analysis. Carbonate powders were reacted with 105% anhydrous phosphoric acid in a common acid bath at the University of Michigan (UM) and

182 analyzed for $\delta^{13}C$, $\delta^{18}O$ and Δ_{47} on a Thermo Scientific MAT 253 Mass Spectrometer following
183 established extraction and data reduction procedures (Defliese et al., 2015; Supplemental
184 Methods). For organic $\delta^{13}C$, carbonate was removed via reaction with weak HCl and analyzed at
185 UM on a Costech Elemental Analyzer attached to a Thermo Delta V. The Δ_{47} values were
186 corrected for the temperature of acid reaction (Defliese et al., 2015) and normalized relative to
187 the Absolute Reference Frame (ARF) of Dennis et al. (2011). Stromatolitic material contains a
188 relatively high abundance of organic matter that can pose a challenge to reliable clumped isotope
189 measurements. Analytical methods ensured samples presented had low Δ_{48} and Δ_{49} values.
190 Isotopic data are included in Tables 1–3. Mean Δ_{47} values of UM Carrara after normalization
191 were 0.397 +/- 0.007 and 0.406 +/- 0.007 during the analytical period. Standard errors for Δ_{47}
192 temperature estimates were ~ 2.6 to 6 °C for unknowns, with the exception of two samples that
193 show considerably higher uncertainty (11.7 °C), possibly due to heterogeneity of the carbonate
194 powder as a result of inclusion of trace amounts of secondary, higher temperature sparite during
195 the micro-drilling process. Reproducibility for conventional carbonate $\delta^{13}C$ and $\delta^{18}O$ and organic
196 carbon $\delta^{13}C$ was better than 0.2‰ for all analyses. All of the measured and calculated
197 geochemical data are presented in Tables 1–3 and raw data in Supplemental Data. We note that
198 all data were collected prior to the establishment of current background and ^{17}O correction
199 procedures (Bernasconi, 2018; Peterson et al., 2019), which can result in higher analytical
200 uncertainties than present.
201
202 **4. Results**
203
204 *4.1 Carbonate geochemistry results*
205
206 Thin section analyses of mat carbonates show finely laminated layers (Figure 3B and C)
207 with organic matter bound, in parts, by coarse-grained, anhedral microsparite that is readily
208 distinguished from laminated carbonate. Stromatolite microfabrics contain light-dark laminae
209 ~20 μm to several millimetres thick and consist of calcite and a mix of detrital material (Elmore,
210 1983, 1984). Mean mat Δ_{47} values range from 0.602 to 0.699, corresponding to temperatures of
211 22 to 44 °C for the Defliese et al. (2015) calibration line (Table 1), which was derived in the
212 Stable Isotope Lab at UM. For reference, temperatures calculated for the same Δ_{47} values were

calculated following the Dennis et al. (2011) calibration line as well (Table 1). The Δ_{47} values for anhedral sparite are lower (0.568 to 0.666), yielding higher formation temperatures of 29–54°C (Defliese et al. 2015). These data show a consistent, but small offset between primary and secondary carbonate Δ_{47}, indicating infilling of void space by secondary calcite after burial. Secondary carbonate may bias primary carbonate material via infilling of microvoids in the carbonate fabric that may be difficult to separate when sampling. The Δ_{47} temperatures are used for two purposes: 1) to provide constraints on potential diagenetic temperatures affecting organic carbon associated with the mats, and 2) to provide reasonable bounds to calculate the $\delta^{18}O$ of fluids in equilibrium with the carbonate using the temperature-dependent fractionation factor (Kim and O'Neil 1997). Δ_{47} temperatures may also provide an upper bound for formation temperature, as secondary processes are unlikely to produce cooler temperatures. The Δ_{47} temperatures and $\delta^{18}O_{carb}$ yield water compositions of -1.7 to -5.4‰ for T °C =25 and 40 °C (Table 3), consistent with a range of fresh meteoric waters at low latitude, although calculated fluid compositions have the potential to be biased by any post-depositional solid state bond reordering that could have affected clumped isotope temperatures.

4.2 Organic geochemistry results

Copper Harbor Conglomerate stromatolites contain 0.04 to 0.22 wt. % organic carbon within carbonate laminae. In areas with no visible recrystallization, it is assumed that this organic matter reflects primary Mesoproterozoic organics, unmodified by any post-depositional thermal processes (see *5.1*). The $\delta^{13}C_{org}$ values range from -24.0 to -27.4‰ (Table 2) and are comparable to $\delta^{13}C_{org}$ from contemporaneous floodplain sedimentary rocks from the MCR (-26 to -29‰; Sheldon, 2012) and enriched compared to Nonesuch Formation kerogen ($\delta^{13}C$ = -30 to -34‰; Imbus et al. 1992). Inorganic carbonate $\delta^{13}C$ values from stromatolite laminae range from -0.8 to -1.9‰ with $\delta^{18}O$ of 23.2 to 24.1‰ VPDB and show little or no variability with position in the mat. Measured CHC carbonate $\delta^{13}C$ values are consistent with $\delta^{13}C_{carb}$ values of carbonates found within the Nonesuch shale and CHC mat carbonates (Imbus et al. 1992). Imbus et al. (1992) note that consistency between CHC mat carbonate $\delta^{13}C$ and Nonesuch layered carbonate $\delta^{13}C$ suggests a common Dissolved Inorganic Carbon (DIC) source for these associated sediments.

5. Discussion

5.1 Preservation potential of Carbonate Δ_{47} During Burial and Sediment Diagenesis

The Δ_{47} data from mat carbonates have the potential to record Mesoproterozoic temperature, however there are a number of potentially significant uncertainties associated with interpreting Δ_{47} data from 1.1 Ga microbial carbonates. This is particularly true when relating measured temperature to environmental conditions at the time of mat formation. Thus, it is suggested that measured Δ_{47} temperatures do not necessarily reflect primary formation temperature, but could record a combination of formation temperature plus secondary effects that bias primary signatures. First, a number of authors have identified deviations from the experimental temperature-Δ_{47} calibration line for equilibrium precipitation (Ghosh et al., 2006) that may result from kinetic isotope effects (Affek et al., 2008; Daëron et al., 2011; Eagle et al., 2013; Ghosh et al., 2006; Saenger et al., 2012; Tripati et al., 2010). This has the potential to influence interpreted carbonate formation temperature. If mat carbonate forms at or near equilibrium, Δ_{47} from CHC mats should yield reliable temperature estimates, barring secondary alteration or solid-state reordering. However, if the carbonates formed via rapid CO_2 degassing (Affek et al., 2008), kinetic effects could decrease recorded Δ_{47} values, producing an increase in apparent temperature. Recent work by Petryshyn et al. (2016) shows that modern microbial mats yield Δ_{47} temperatures within error of summer water temperature for non-diagenetically altered carbonates. However, ancient mat carbonates from the Eocene Green River Formation (Frantz et al., 2014) are also shown to reproduce surface water temperatures reasonably well. Thus, while the extent of kinetic bias on temperature relationships are at present unknown, microbial carbonate temperatures recorded by carbonate Δ_{47} are generally consistent with modern environmental conditions, but represent at best a seasonal maximum. This result is similar to Δ_{47} in other lacustrine carbonates that are shown to record warm season temperatures (Hren and Sheldon 2012).

Second, solid-state bond reordering has the potential to alter Δ_{47} values over 1.1 Ga and at moderate temperatures (Henkes et al., 2014). This becomes a greater probability with increasing burial temperature and time. Thus, Δ_{47} values from Proterozoic carbonates should be

275 viewed cautiously as a record of primary T °C and most likely represents a combination of
276 primary temperatures and an unknown degree of thermal reordering. For CHC stromatolites,
277 potential post-depositional Δ_{47} alteration is likely minimized by low burial depths and
278 temperatures. The coolest stromatolitic Δ_{47} temperatures measured are <30 °C and mean sparite
279 Δ_{47} temperatures are all lower than 54 °C. Clumped isotope temperatures therefore likely show
280 minor thermal alteration during shallow burial heating since the Mesoproterozoic. Biomarker and
281 clay mineral thermometry support low regional MCR burial temperatures (100–125 °C)
282 (Nishioka et al., 1984; Pratt et al., 1991), but far warmer than measured mat Δ_{47} values. Regional
283 temperatures from clay and biomarker data are consistent with recent clumped isotope results
284 from the MCR White Pine Mine, that show spatially variable hydrothermal temperatures (49–
285 116°C) in association with zones of copper mineralization, and fluid inclusions show
286 equilibration temperatures of 53–88°C (Nishioka et al. 1984). If the MCR experienced
287 prolonged periods of high temperature (>125 °C) for tens of millions of years, this could have
288 the effect of resetting primary Δ_{47} results to lower values (higher T °C) (Gallagher et al., 2017).
289 The highest measured Δ_{47} temperatures in the MCR are found in areas with obvious alteration of
290 primary carbonate and closest to the major bounding Keweenaw Fault. Results from altered CHC
291 carbonates relatively close to the Keweenaw Fault, show the lowest Δ_{47} temperatures of the
292 MCR even within the alteration zone (~70°C; Gallagher et al., 2017). The sample location of
293 Horseshoe Harbor, well-removed from the Keweenaw Fault, suggests that it is within one of the
294 lowest thermal alteration zones of the whole MCR and thus would be expected to have the least
295 thermal impact from either burial or primary ore-related fluids. This is supported by fluid
296 inclusion data that shows the lowest closure temperatures are found within mat carbonates at
297 Dan's point, near the sampling locality used for this paper (Nishioka et al. 1984). In the absence
298 of recrystallization, post-depositional alteration is expected to decrease bond ordering (Henkes et
299 al., 2014) and Δ_{47} values, resulting in higher calculated temperatures. Bond-reordering
300 experiments predict that the Δ_{47} temperatures preserved by stromatolites could in fact reflect
301 primary or early diagenetic crystallization temperature (Henkes et al., 2014; Shenton et al.,
302 2015). Regardless, the low temperatures recorded in mat carbonate Δ_{47} suggest minimal
303 temperature effects due to bond reordering.
304 In addition to effects of bond reordering, shallow-water carbonate diagenesis can
305 introduce alteration of primary geochemical signatures within ancient carbonates (Ahm et al.,

2018; Higgins et al., 2018). In particular, variations in the extent and style of early diagenesis can influence whether the composition of the carbonate mineral is determined by chemistry of the fluid or by the precursor sediment. This results from the fact that the transformation of metastable carbonate minerals to more recalcitrant forms such as limestone or dolomite, involves exchange between mineral and pore-fluids that can translate to fluid-buffered exchange for one element such as O and sediment buffered for another such as C (Higgins et al., 2018). Indeed Swart (2008) argues that stratigraphic variations in Neogene marine carbonate $\delta^{13}C$ could be explained, in part, due to mixing of pelagic and platform C sources with distinct $\delta^{13}C$ values. Higgins et al. (2018) suggest that observed Neogene carbonate $\delta^{13}C$ trends could reflect changes in the extent of diagenetic alteration of aragonite to calcite under fluid-buffered conditions. Thus, changes in relative sea level could in fact account for much of the variability in the Neogene marine $\delta^{13}C$ record.

CHC stromatolites are comprised of primary calcite microlaminae in association with secondary sparite outside the mat. Early diagnetic transformation of metastable carbonate phases to more stable calcite could bias the carbon isotope signature preserved in these samples if the process occurred under fluid- versus sediment-buffered conditions. Carbon is typically assumed to be robust to diagenetic alteration due to sediment buffering of a carbonate-rich system. This contrasts with oxygen, which is more likely to be fluid-buffered due to the relative abundance of water during diagenesis. High burial temperatures could result in significant degradation of sedimentary organic matter associated with thermal cracking and shift the DIC pool closer to organic-derived carbon sources. Carbonate $\delta^{13}C$ and $\delta^{18}O$ values for CHC mat calcite and secondary sparite are similar despite different modes and timescales of genesis, with no consistent relationship between Δ_{47}, $\delta^{13}C$, and $\delta^{18}O$ data. While one cannot exclude fluid-buffering of the carbon pool during any transformation of metastable mat carbonate to calcite, it is assumed here that mats represent primary or sediment buffered conditions for carbon and either sediment or fluid buffered system for oxygen.

Due to the 1.1 Ga age of the CHC, Δ_{47} values of non-recrystallized primary carbonate most likely represent a mixed primary and secondary signature. Processes of non-equilibrium kinetic isotope fractionation and diagenetic alteration of primary carbonate after formation are all expected to yield temperatures higher than conditions during formation, as there is no convincing mechanism for producing colder temperatures via secondary processes after burial. Thus, while

other geochemical studies such as magnetic susceptibility (Petryshyn et al., 2016) could potentially provide additional constraints on the extent of possible diagenetic alteration of primary carbonate for the CHC mats, it is believed that the low temperatures preserved in stromatolitic carbonate record maximum crystallization temperature at or soon after formation. There is no simple scenario to explain the generation of cooler Δ_{47} temperatures due to burial for a billion years and briefly, at temperatures up to 125°C. Thermal history modelling of the MCR indicates that for a carbonate formed at 25°C, temperatures >140°C would be required to alter clumped isotope temperatures by more than +10°C, with no increase in apparent clumped temperature for burial at 125°C (Gallagher et al. 2017). Thus, because the maximum alteration temperatures were at or below that threshold, Δ_{47} data could provide a maximum T °C of the palaeoenvironment but no information on whether or not conditions were significantly cooler than this. These data do indicate, however, that the mat carbonates did not experience enough heating to fully reset clumped isotope data.

Despite uncertainty in the absolute temperature of formation, Δ_{47} data record a maximum formation temperature of less than 30°C. The low temperatures recorded by stromatolite carbonate within the CHC as well as associated sparite suggests that organic carbon occluded within these same layers also likely did not experience significant thermal degradation or recrystallization associated with higher burial temperatures. Significant alteration of kerogen $\delta^{13}C$ values only occurs at much higher temperatures (>500°C; Peters et al., 1981; Schoell, 1984), and abiogenic generation of isotopically depleted values requires both high temperature and high pressure (McCollom and Seewald, 2006). Based on this, it is assumed that neither carbonate nor organic matter carbon isotopic compositions are likely to have been altered dramatically from primary compositions.

5.2 Stromatolite Organic Matter, Carbon isotopes, and Implications for Mesoproterozoic pCO_2

A number of authors have used organic $\delta^{13}C$ data to quantify the concentration of dissolved inorganic carbon (Eichmann and Schidlowski, 1975; Popp et al., 1989), most commonly with free-floating aquatic organisms that can take up aqueous CO_2 directly from the surrounding water. This approach is founded on the observation that autotrophic photosynthetic

carbon fixation involves transport of inorganic carbon to the site of fixation and binding with the C-fixing enzyme (Farquhar et al., 1982; O'Leary, 1981). In aqueous environments and for organisms without active CO_2 transport, the $\delta^{13}C$ of fixed carbon is controlled by the rate of diffusion of CO_2 to the fixation site and the isotopic composition of the dissolved $CO_{2(aq)}$ pool. The overall isotope effect can be described by:

$$\varepsilon_p = \varepsilon_t + (\varepsilon_f - \varepsilon_t)p_i/p_a \quad (1)$$

where ε_p equals the isotope effect associated with C fixation, ε_t = fractionation associated with CO_2 diffusion (ε_{tw} = -0.7 ‰ in water), ε_f = isotopic fractionation associated with C fixation by the Rubisco enzyme (~ -29‰), and p_i and p_a reflect the internal and ambient pCO_2 (Farquhar et al., 1982; O'Leary, 1981; Popp et al., 1989). Such an approach provides a reasonable estimate of the effect of carbon limitation (i.e. concentration) on isotope discrimination.

In an aqueous system, the isotope effect can be described by $\varepsilon_p = ([\delta_p + 1000)/(\delta_d + 1000]-1)*1000$ where δ_p represents organic fixed carbon and δ_d the DIC. The $\delta^{13}C_{aq}$ is recorded by $\delta^{13}C_{carb}$, and follows the temperature-dependent fractionation between DIC and calcite (Deines et al., 1974). The $\delta^{13}C_{org}$ represents δ_p and is paired with $\delta^{13}C_{DIC}$ to quantify carbon isotope discrimination during biosynthetic C fixation. Inorganic carbonate $\delta^{13}C$ may be related to $\delta^{13}C_{CO2\ aq}$ using the temperature-dependent fractionation between $CO_{2(g)}$ and $CO_{2(aq)}$ (Deines et al., 1974).

The CHC microbial mats were formed in a braidplain system (Elmore 1983,1984; Sheldon, 2012, Wilmeth et al., 2014; Petryshyn et al. 2015; Fedorchuk et al. 2016) and preserve ancient organic carbon, as well as mat-associated carbonate. As a result, these systems record the isotopic composition of fixed organic carbon and the dissolved inorganic carbon that may have been utilized for C fixation during growth in these systems. Microbial mats present a more complex system with respect to carbon cycling/diffusion than individual free-floating cellular organisms, yet the fundamental principles of carbon discrimination remain unchanged. Mats can be treated effectively as an ecosystem that ultimately is limited by the same factors (carbon, major and minor nutrients, nitrogen, and available chemical or light energy) as a single cell. Mat organic carbon and carbonate $\delta^{13}C$ are used to provide bounds on carbon discrimination during mat formation that can be related to general carbon limitation. For photoautotrophs, this is

ultimately limited by the dissolved inorganic carbon pool, which in many cases is controlled by atmospheric pCO_2. The $\delta^{13}C_{calcite}$ is used to constrain $\delta^{13}C_{aq}$ following Deines et al. (1974) using an assumed temperature of 25 and 40°C. These temperatures are consistent with surface conditions proposed by Fiorella and Sheldon (2017) for these palaeolatitudes under a variety of greenhouse gas scenarios, as a plausible but poorly constrained palaeotemperature. Reconstructed clumped isotope temperatures from the CHC stromatolites of 22–44° C provide some additional support for this range of potential mat environmental conditions. Mean $\delta^{13}C_{aq}$ values range from -10.8 at 25°C to -9.6‰ at 40°C (Table 3). Combined with mean organic carbon $\delta^{13}C$ of stromatolite laminae (-25.8‰), these data yield calculated ε_p values of 15.4 to 16.7. If the the most depleted organic carbon isotope values represent the primary $\delta^{13}C_{org}$, absolute ε_p values for CHC mats range from 17.1 to 18.4.

Stromatolite carbon isotopes and ε_p can be related to dissolved inorganic carbon concentrations (DIC) and ultimately ambient CO_2 if 1) the mechanisms of carbon fixation/mat formation are known and 2) modern isotope systematics show a relationship to ambient CO_2 in the environment of formation. A variety of mechanisms drive the formation of carbonate within stromatolitic mats (Dupraz et al. 2009), including uptake of CO_2 during photosynthesis and degassing of CO_2 from waters. Depending on the formation environment, aqueous systems may be in varied states of CO_2 disequilibrium relative to the atmosphere. The CHC mats are draped over large cobbles, formed on conglomeratic lenses, and infilled with sands, gravels, and silts associated with the alluvial fan of the Mesoproterozoic Rift (Figure 2). Associated with these stromatolites are intact mud-cracks and ripples, some containing gypsum, as well as recognized exposure surfaces (Elmore, 198, 1984) that indicate a shallow, episodically sub-aerial, and variable-energy aqueous system. CHC mats were formed in shallow water, within the photic zone. In addition, acritarchs found in associated sediments (Wellman and Strother, 2015) and carbon isotopes of organic matter within the CHC mats and penecontemporaneous floodplain mats (Sheldon, 2012) strongly suggest phototrophy as a key metabolism. Thus, it is highly probably that CHC mat carbon fixation was underpinned by phototrophic metabolism. Growth waters were likely at least somewhat mixed with respect to the atmosphere. Environments characterized by high shear stress have potential to inhibit microbial mat accumulation, thus mat structures preserved in the CHC could have formed during intervals of greater quiescence within an otherwise turbid system (Elmore, 1983). Such conditions would be more prone to restriction,

with mat accumulation representative of low energy intervals. However, regular intermixing of coarse sand and sediment as well as large cobbles within mat layers indicate frequent intervals of turbidity were likely a regular feature of the system (Fig. 2c). Furthermore, direct association of mats with ripples strongly support growth in an environment with moving water that is likely to have greater exchange of dissolved gases between the aqueous environment and the atmosphere.

The second condition that must be met to relate mat carbon isotopes to ambient CO_2 is that modern mats must show a relationship between DIC, pCO_2, and carbon discrimination. Chemostat experiments show that ε_p of photosynthetic autotrophs is controlled by dissolved CO_2, nutrient availability, growth rate, and for single cells, cellular volume to surface area ratio (V/S) (Dupraz et al., 2009; Laws et al., 1995; Popp et al., 1989) (Figure 4). In a well-mixed water body, the $\delta^{13}C_{org}$ of individual aquatic photosynthesizers reflects isotopic discrimination associated with diffusion of CO_2 to the site of C fixation and the dissolved CO_2 is proportional to atmospheric pCO_2. In biogenic stromatolitic mats, fine scale carbon isotope systematics are highly variable with depth in the mat due to unique assemblages of symbiotic organisms and restrictions on gas diffusion through the mat. Despite these complexities, empirical data show that just as for free-floating aquatic organisms, the amount of dissolved CO_2 in water is generally the first order C limitation for photoautotrophs within a mat. This limitation is in part recorded in the biomass $\delta^{13}C$ of mat ecosystems, which integrate material from chemoautotrophs or photoautotrophs and the heterotrophs that feed on them or their exudates. As with single-celled organisms, modern empirical data show that bulk mat ε_p approaches a maxima when pCO_2 or dissolved CO_2 is high in the aqueous environment (Figure 4). This empirical observation provides an important, if imperfect tool to assess past pCO_2, particularly when estimates for atmospheric pCO_2 range from several times PAL to >100x PAL.

Studies of carbon isotope fractionation during CO_2 uptake and photosynthetic fixation show a strong dependence on dissolved aqueous CO_2 concentration (Popp et al., 1989). Under conditions of low $CO_{2\ aq}$ and $pCO_{2\ atm}$, $\delta^{13}C$ of organic biomass shows significantly reduced carbon isotope discrimination, while under high CO_2 availability, carbon isotope discrimination approaches a theoretical maximum (Popp et al., 1989). Data from modern microbal mat carbonates formed in marine hypersaline, freshwater alkaline, and hydrothermal systems were used to calculate carbonate isotope discrimination (ε) as a function of variable [DIC] using published $\delta^{13}C_{carbonate}$, $\delta^{13}C_{mat}$, and DIC data (Brady et al., 2013; Des Marais et al., 1992; Pagès

et al., 2014). The ε value is calculated after Laws et al. (1995), where $\varepsilon = (1000*(\delta^{13}C_{org}-\delta^{13}C_{aq})/(1000+\delta^{13}C_{org}))$. For clarification, the $\delta^{13}C$ of organic matter was compared relative to $\delta^{13}C_{aq}$ (not $\delta^{13}C_{DIC}$) to quantify ε. The $\delta^{13}C_{gas}$ was calculated from the isotopic composition of associated carbonates using the empirical $\delta^{13}C_{carb}/\delta^{13}C_{aq}$ fractionation factor determined by Deines et al. (1974). Figure 4 shows measured ε vs $CO_{2\ aq}$ for modern microbial mats in alkaline pools in British Columbia (Brady et al., 2014), Orakei Hot Springs (Des Marais et al., 1992), and Shark Bay (Pages et al., 2014), as well as data for free-floating single cell growth experiments (Laws et al. 1995; McCabe, 1985), and the pCO_2 that would be calculated for an atmosphere in equilibrium with the dissolved $CO_{2\ aq}$. These data provide boundary conditions for examining the isotopic values recorded by CHC mat carbonate and organic matter. The pCO_2 values associated with each ε value for modern mats do not represent true atmospheric pCO_2, but rather the calculated pCO_2 based on the measured dissolved CO_2 concentration (DIC in μmol L^{-1}), water temperature, Henry's constant for CO_2, and assumption of equilibrium between DIC and the atmosphere. Using this approach, the calculated atmospheric pCO_2 for waters associated with carbonate-bearing microbial mats in British Columbia (Brady et al., 2014) range from 93 to 413 ppm with a mean of 208 ppm. Modern data for Orakei hot springs have high DIC and high CO_{2aq} and are not in equilibrium with the atmosphere due to high dissolved CO_2. These produce a theoretical $pCO_{2\ atm}$ value significantly in excess of modern and are included to demonstrate that waters in equilibrium with far higher dissolved CO_2 concentrations than the modern still follow the general patterns of carbon isotope discrimination observed in other mat systems. The modern mat C data shown here is derived from environments with flowing water, lakes, and marine systems, with mixed microbial communities. All follow the general relationship between [DIC] and carbon isotope discrimination within the mat.

Modern mats exhibit smaller ε_p than plants or single celled photoautotrophs for comparable pCO_2, likely due to diffusion limitation at the water-mat interface, C-limited cellular growth rates, and recycling of C within the mat system. The difference is greatest in modern mats in hypersaline or high temperature conditions where ε_p values may range from ~1–14 for a range of dissolved aqueous CO_2. Stromatolitic mats today are characterized by complex cycling of carbon that varies as a function of microbial assemblages and aqueous conditions. Thus, it is known that there can be significant variation in CO_{2aq} and $\delta^{13}C_{org}$ within a mat and between different mat types (Dupraz et al., 2009). This heterogeneity was likely no different in the deep

492 past. For example, Lepot et al. (2009) show large variability in $\delta^{13}C$ of organic matter in 2.72 Ga
493 microbial structures, highlighting the role of microbial metabolism in controlling isotope
494 heterogeneity on the micron scale and larger. Despite this, microbial mats are ecosystems
495 comprised of an array of communities assembled into effectively a single structure. All
496 organisms within this system are ultimately limited by one or more nutrients, including carbon.
497 From an ecosystem perspective, modern data provide semi-quantitative boundary conditions for
498 interpreting ancient mat systems, particularly when considering ancients systems for which some
499 suggest pCO_2 was in excess of 30–100x PAL. Modern data demonstrate that for most shallow
500 mat systems within the photic zone with a significant proportion of phototrophs, mats as a whole
501 are sensitive to large changes in $CO_{2\,aq}$, producing a large increase in ε for only modest increases
502 in $CO_{2\,aq}$. A mat within a mixed aquatic system can effectively be thought of as a system with a
503 very large volume to surface area ratio (surface area being the exposed interface between the mat
504 and ambient water), whereas under quieter conditions, effective volume to surface area would be
505 lower. Modern mat isotope data match reasonably well (Figure 4) with CO_2-carbon isotope
506 sensitivity observed in modern free-floating low volume to surface area microbes with slow
507 growth rate (Laws et al., 1995; McCabe, 1985).
508 One potential complication to the approach used here to constrain past DIC and
509 ultimately pCO_2, is if CO_2 was not the primary C source supporting the mat system. For
510 example, Olsen et al., (2016) suggest that marine methanotrophy coupled with sulfate reduction
511 could have been an important component of C and S cycling in the Mesoproterozoic, serving as a
512 limit to buildup of CH_4 in the atmosphere. If the mat ecosystem was dominated by
513 methanotrophy with CH_4 available via sources outside the mat, this would render expected
514 relationships between mat $\delta^{13}C$ and atmospheric pCO_2 (by virtue of the relationship with DIC)
515 void. Methanotrophs can derive energy via either anaerobic or aerobic pathways. In the modern,
516 mats underpinned by anaerobic methanotrophy are observed in areas of methane and other
517 hydrocarbon seeps and often asscoated with sulfate reduction (Drake et al., 2015). In benthic
518 mats near seeps, methanotrophy may contribute nearly 50% of total fatty acids in mat organics
519 (Ding and Valentine, 2008). However, CHC mats are located in a relatively shallow ancient
520 braidplain and are associated with mudcracks and gypsum, indicating at least somewhat oxic
521 conditions and free sulfate at or around the time of mat formation. In addition, anaerobic
522 methanotrophy is known to generate some of the most depleted $\delta^{13}C$ values in carbonate (-

125‰; Drake et al., 2015). While it is impossible to rule out methanotrophy as an important metabolism within CHC mats, fossil evidence of phototrophs and $\delta^{13}C$ data are consistent with phototrophy.

Carbonate and organic $\delta^{13}C$ data from CHC stromatolites are coupled with clumped isotope temperatures to provide reasonable boundary conditions for $\delta^{13}C_{CO2aq}$, ε_p, and CO_{2aq}. Because mat samples derive from a system with at least intermittently moving water (Figure 2) and underlain by non-carbonate bedrock, it is assumed that limitation to CO_2 diffusion into or out of the water system is far less than within the mat system. Thus, even in slow or occasionally stagnant water, CO_2 diffusion into the mat is likely the primary limitation to carbon assimilation within the mat as a whole. With these assumtions, modern data provide reasonable, if imprecise limits for interpreting palaeo-ε data with respect to ancient $CO_{2\ aq}$ and pCO_2 within the palaeo-environment. Specifically, carbon discrimination data from modern hot springs is used as an upper limit for ε_p-pCO_2 relationships in the ancient. Measured ε_p values for the Proterozoic stromatolites range from 15.4 to 18.4 for temperatures of 25 to 40°C. Modern mat ε_p values are all less than 21‰ and mats that record an ε_p of less than 18‰ are found in waters in equilibrium with DIC of less than 130 μM, consistent with a pCO_2 effectively less than 1000 ppm. Modern mat carbon discrimination data generally follows the pattern of ε_p versus DIC observed in slow growing cells with moderate to high volume to surface area (Figure 4). The ε_p data for CHC mats are equivalent to modern mats grown in waters with DIC and in theoretical equilibrium with pCO_2 of less than ~20x PAL, and most consistent with mat data for waters in equilibrium with pCO_2 of less than several times PAL. While pCO_2 estimates based on $\delta^{13}C_{org}$-$\delta^{13}C_{DIC}$ requires accurate measurement of primary $\delta^{13}C_p$ and $\delta^{13}C_{aq}$ and optimally, equilibrium between the DIC and the atmosphere, these limits are consistent with palaeosol (Sheldon, 2006, 2013), single organism carbon discrimination (Kaufman et al., 2003), and fossil carbonate-based (Bartley and Kah, 2004; Kah and Riding, 2007) estimates for late Mesoproterozoic pCO_2 (Figure 5). Thus, CHC stromatolite data are consistent with both temperate palaeoenvironmental conditions and relatively low pCO_2.

5.3 Comparison of Temperature, pCO_2 and Mesoproterozoic AOGCMs

Reconstructions of past solar insolation indicate that a "faint young Sun" paradox exists throughout the Precambrian wherein equable conditions would need to have been maintained in the presence of significantly lower insolation that has increased steadily from less than 70% of the present day value over the past 4.5 Ga (Gough, 1981). Recent work by Fiorella and Sheldon (2017) using 91% total solar insolation (Gough, 1981) shows that an equable Mesoproterozoic climate could have been maintained by increased CH_4 flux from methanogenic bacteria even in the absence of strongly elevated pCO_2. The AOGCM outputs show that ice-free conditions could be maintained for pCO_2 <10x PAL with the threshold for regional-scale glaciation occurring with CH_4 at 28 ppmv or pCO_2 below 5x PAL. These results are in agreement with temperatures for ~30° latitude predicted by AOGCM simulations of the Mesoproterozoic using these boundary conditions (Figure 6). Recent work by Olson et al. (2016) suggests that anaerobic oxidation of CH_4 coupled with SO_4^{2-} reduction could act as an obstacle to CH_4 accumulation in the atmosphere, limiting pCH_4 to less than 10 ppmv if the only source of CH_4 is marine production, independent of pO_2. If both the AOGCM results (Fiorella and Sheldon, 2017) and modeled CH_4 fluxes are correct (Daines and Lenton, 2016; Olson et al., 2016), a paradox develops because the apparent CH_4 level would be too low to support the observed equable conditions.

There are at least two potential solutions to this paradox. The first is that a marine-only model of CH_4 flux underestimates the total biogenic CH_4 flux. As noted above, there is extensive evidence for a significant lake and floodplain biosphere (Elmore, 1983; Sheldon, 2012; Wellman and Strother, 2015) by the Mesoproterozoic and many stable isotopic values from those systems, especially in palaeo-lake sediments (Imbus et al. 1992), are too negative to have been the result of C derived only from photosynthetic means. Thus, a potentially large terrestrial biogenic CH_4 flux is supported by existing constraints. This idea was recently tested by Zhao et al. (2017) who modeled the potential for a significant terrestrial CH_4 flux to supplement the marine CH_4 flux. They found that if terrestrial cyanobacterial mats covered 8–10% of the Earth's surface, clement conditions would have been maintained even at the relatively low pCO_2 values indicated by palaeosols (Sheldon, 2013) and, as reported herein, microbialites.

Secondly, atmospheric model simulations have typically focused on a narrow range of greenhouse gases that include CO_2, CH_4, and sometimes, H_2O vapour (cf. Roberson et al., 2011). However, there are a number of other greenhouse gases that have significantly higher climate forcings than CO_2 that are poorly constrained in the geologic record. For example, as Fiorella

and Sheldon (2017) noted, one potential way to reconcile differences in CH_4 levels is with N_2O (see Roberson et al. (2011) for an example). While there are no direct proxies for pN_2O, a ten-fold increase from the modern value of 0.3 ppm would provide enough additional greenhouse forcing to offset a five-fold lower pCH_4 value. Thus, there are at least two potential solutions to the apparent CH_4 paradox that would bear further investigation. Ultimately, development of proxies for greenhouse gases beyond CO_2 would substantially enhance our ability to reconcile the challenges presented by the "faint young Sun" paradox across the whole of the Precambrian.

6. Conclusions

Sedimentary features and organic and inorganic carbon isotope data from 1.1. Ga stromatolites in the Copper Harbor Conglomerate indicate formation in waters with relatively low DIC. This most likely results from equilibrium with a relatively low atmospheric pCO_2 (less than 20x PAL; Figures 4 and 5) during a time when solar luminosity was ~9% lower than today. If pCO_2 was indeed lower than this bound, elevated concentrations of other greenhouse gases such as methane, may have played a role in regulating global temperature. However, current estimates of the potential Mesoproterozoic CH_4 flux from marine environments are relatively low, creating a methane paradox. The paradox is potentially resolvable either through a relatively extensive terrestrial biosphere or through elevated levels of other greenhouse gases such as N_2O. At present, the means to test between those hypotheses is lacking, but if biologically-produced gases such as CH_4 played a key role in regulating global temperature during the Mesoproterozoic, their concentrations may have acted as a negative feedback to the buildup of atmospheric O_2 due to the potential to oxidize readily in the presence of free oxygen as well as providing global climate regulation.

Acknowledgements

This work was supported in part by University of Michigan Turner Postdoctoral Fellowship funding to MTH and NSF EAR 1050760 to NDS.

Appendix A. Supplementary data

Supplementary data associated with this article can be found in the online version, at http:XXXXXXX.

Figure Captions

Figure 1. Location map for Copper Harbor Conglomerate on the Keweenaw Peninsula, Michigan, USA. Samples were collected from Horseshoe Harbor and pCO_2 estimates from that site are compared to estimates from a palaeosol at Sturgeon Falls (MI) and from palaeosols in the North Shore Volcanic Group (NSVG; inset map). Figure modified after Mitchell and Sheldon (2016).

Figure 2. Field photos of Copper Harbor Conglomerate stromatolites. Image of (A) stromatolite mats growing on large cobbles (B) infilled by coarse-grained sands, (C) with cobbles and gravel entrained within the mat, and (D) growing on cobbles and sandy beds and with entrained sand layers.

Figure 3. Field and thin section photos of Copper Harbor Conglomerate stromatolites. (A) Stromatolite mat overlain by coarse-grained sandstone deposited in a fluvial setting. (B) Thin-section image of finely laminated mat with mineral grains embedded in the mat matrix. (C) Thin section image of the top of a mat layer, bounded by secondary sparite.

Figure 4. Carbon isotope discrimination (ε_p) between mat organic matter and $CO_{2(aq)}$ for modern microbial mats from alkaline, evaporative marine, and hydrothermal systems. For reference, ε_p data and predictions for single celled aquatic organisms as a function of CO_2

646 $_{(aq)}$ are shown. Solid lines represent the empirically-derived relationships between C
647 isotope discrimination and $CO_{2\,(aq)}$ for single celled organisms with a volume to surface
648 area (V/S) ratio of 5 and varied growth rates ($\mu\ d^{-1}$) after Laws et al. (1995). Gray shaded
649 area shows the calculated ε_p values for CHC mats. The CHC mats yield ε_p values
650 compatible with modern mats in waters with low $CO_{2\,(aq)}$, and fall below the empirical
651 relationship for slow growing photoautotrophs ($\mu = 0.2$) with moderate to high V/S ratios.
652 The ε_p data are compatible with mats formed in waters with $CO_{2\,(aq)}$ that is equivalent to
653 less than ~20x PAL, and most consistent with Mesoproterozoic pCO_2 of less than several
654 times PAL.
655
656 Figure 5. Proterozoic pCO_2 ranges. Gray shaded area shows upper and lower pCO_2 limits
657 for an ice-free (20 °C) and glacial (5 °C) world based on photochemical model estimates
658 (Kasting, 1987). Calculated pCO_2 estimates (<20x PAL and most likely <5x PAL) agree
659 with (A) cyanobacterial calcification (Kah and Riding 2007), (B) minimum isotopic
660 (Kaufman and Xiao 2003), (C) palaeosol mass balance (Mitchell and Sheldon, 2010;
661 Sheldon 2006; 2013), and (D) carbon reservoir modelling (Bartley and Kah 2004)
662 estimates. These data support equable Mesoproterozoic temperatures and low pCO_2. These
663 data indicate that CH_4 or some other greenhouse gas (e.g. N_2O) likely played a role in
664 regulating global temperature and provided a negative feedback to the buildup of
665 atmospheric oxygen (figure modified from Kah and Riding, 2009).
666
667 Figure 6. Calculated zonal mean temperatures for the Mesoproterozoic using boundary
668 conditions of 5x PAL CO_2 (bottom line) and 10x PAL and 140 ppm CH_4 (top line) and
669 Mesoproterozoic palaeogeography (Fiorella and Sheldon, 2017). Upper boundary for
670 Mean Annual Air Temperature (MAAT) for the tropics and/or near tropical regions (<30°
671 latitude) is shown (circle and shaded area) based on stromatolite Δ_{47} temperature data that
672 may reflect a combination of primary and/or early diagenetic alteration of original clumped
673 isotope signatures.
674
675 Table 1. The Δ_{47} data from stromatolite samples.

676 Table 2. The $\delta^{13}C$ values of occluded organic matter within mats.

677 Table 3. Calculated carbon isotope discrimination for CHC mats.

678

679 **Supplemental Tables and Figures**

680 Figure 1. Heated gas calibration line.

681 Supplemental File 1. Heated Gas Data

682

683 **Conflict of Interest Statement:** The authors certify that they have no affiliations with or
684 involvement in any organization or entity with any financial interest, or non-financial interest in
685 the subject matter or materials discussed in this manuscript.
686
687

688

689

690 **References**

691 Affek, H.P., Bar-Matthews, M., Ayalon, A., Matthews, A., Eiler, J.M., 2008. Glacial/interglacial
692 temperature variations in Soreq cave speleothems as recorded by "clumped isotope"
693 thermometry. Geochim. Cosmochim. Acta 72, 5351–5360.
694 Ahm, A.-S. C., Bjerrum, C. J., Swart, P. K.,Higgins, J. A. 2018. Quantifying early marine
695 diagenesis in shallow-water carbonate sediments. 236, 140-159.
696 Bartley, J.K., Kah, L.C., 2004. Marine carbon reservoir, C_{org}-C_{carb} coupling, and the evolution of
697 the Proterozoic carbon cycle. Geology 32, 129–132.
698 Beghin, J., Storme, J-Y., Blanpied, C., Gueneli, N., Brocks, J.J., Poulton, S.W., Javaux, E.J.,
699 2017. Micro fossils from the late Mesoproterozoic-early Neoproterozoic Atar/El Mreiti
700 Group, Taoudeni Basin, Mauritania, northwestern Africa. Precambrian Research 291, 63–
701 82.
702 Bernasconi, S.M., Müller, I.A., Bergmann, K.D., Breitenbach, S.F.M., Fernandez, A., Hodell,
703 D.A., Jaggi, M., Meckler, A.N., Millan, I., Ziegler, M. 2018. Reducing uncertainties in

carbonate clumped isotope analysis through consistent carbonate-based standardization. Geochem. Geophys. Geosyst. 19,2895-2914.
Brady, A.L., Druschel, G., Leoni, L., Lim, D., Slater, G.F., 2013. Isotopic biosignatures in carbonate-rich, cyanobacteria-dominated microbial mats of the Cariboo Plateau, BC. Geobiology 11, 437–456.
Cannon, W.F., Hinze, W.J., 1992. Speculations on the origin of the North American Midcontinent rift. Tectonophysics 213, 49–55.
Clayton, J.L., Bostick, N.H., 1985. Temperature effects on kerogen and on molecular and isotopic composition of organic matter in Pierre Shale near an igneous dike. Organic Geochemistry 10, 135–141.
Cumming, V.M., Poulton, S.W., Rooney, A.D., Selby, D., 2013. Anoxia in the terrestrial environment during the late Mesoproterozoic. Geology 41, 583–586.
Daëron, M., Guo, W., Eiler, J., Genty, D., Blamart, D., Boch, R., Drysdale, R., Maire, R., Wainer, K., Zanchetta, G., 2011. 13C18O clumping in speleothems: Observations from natural caves and precipitation experiments. Geochim. Cosmochim. Acta 75, 3303–3317.
Daines, S.J., Lenton, T.M., 2016. The effect of widespread early aerobic marine ecosystems on methane cycling and the Great Oxidation. Earth Planet. Sci. Lett. 434, 42–51.
Davis, D.W., Paces, J.B., 1990. Time resolution of geologic events on the Keweenaw Peninsula and implications for development of the Midcontinent Rift system. Earth Planet. Sci. Lett. 97, 54–64.
Defliese, W.F., Hren, M.T., Lohmann, K.C., 2015. Compositional and temperature effects of phosphoric acid fractionation on Δ47 analysis and implications for discrepant calibrations. Chem. Geol. 396, 51–60.
Deines, P., Langmuir, D., Harmon, R.S., 1974. Stable carbon isotope ratios and the existence of a gas phase in the evolution of carbonate ground waters. Geochim. Cosmochim. Acta 38, 1147–1164.
Dennis, K.J., Affek, H.P., Passey, B.H., Schrag, D.P., Eiler, J.M., 2011. Defining an absolute reference frame for “clumped” isotope studies of CO2. Geochim. Cosmochim. Acta 75, 7117–7131.
Des Marais, D.J., Bauld, J., Palmisano, A.C., Summons, R.E., Ward, D.M., 1992. The biogeochemistry of carbon in modern microbial mats. The proterozoic biosphere: a

multidisciplinary study. Cambridge University Press, Cambridge, United Kingdom 299–308.

Douglas Elmore, R., Milavec, G.J., Imbus, S.W., Engel, M.H., 1989. The Precambrian nonesuch formation of the North American mid-continent rift, sedimentology and organic geochemical aspects of lacustrine deposition. Precambrian Res. 43, 191–213.

Dupraz, C., Reid, R.P., Braissant, O., Decho, A.W., Norman, R.S., Visscher, P.T., 2009. Processes of carbonate precipitation in modern microbial mats. Earth-Sci. Rev. 96, 141–162.

Eagle, R.A., Eiler, J.M., Tripati, A.K., Ries, J.B., Freitas, P.S., Hiebenthal, C., Wanamaker, A.D., Jr., Taviani, M., Elliot, M., Marenssi, S., Nakamura, K., Ramirez, P., Roy, K., 2013. The influence of temperature and seawater carbonate saturation state on ^{13}C–^{18}O bond ordering in bivalve mollusks. Biogeosciences 10, 4591–4606.

Eichmann, R., Schidlowski, M., 1975. Isotopic fractionation between coexisting organic carbon—carbonate pairs in Precambrian sediments. Geochim. Cosmochim. Acta 39, 585–595.

Elmore, R.D., 1984. The Copper Harbor Conglomerate: A late Precambrian fining-upward alluvial fan sequence in northern Michigan. Geol. Soc. Am. Bull. 95, 610–617.

Elmore, R.D., 1983. Precambrian non-marine stromatolites in alluvial fan deposits, the Copper Harbor Conglomerate, upper Michigan. Sedimentology 30, 829–842.

Farquhar, G.D., O'Leary, M.H., Berry, J.A., 1982. On the Relationship Between Carbon Isotope Discrimination and the Intercellular Carbon Dioxide Concentration in Leaves. Funct. Plant Biol. 9, 121–137.

Fedorchuk, N.D., Dornbos, S.Q., Corsetti, F.A., Isbell, J.L., Petryshyn, V.A., Bowles, J.A., Wilmeth, D.T., 2016/4. Early non-marine life: Evaluating the biogenicity of Mesoproterozoic fluvial-lacustrine stromatolites. Precambrian Res. 275, 105–118.

Finnegan, S., Bergmann, K., Eiler, J.M., Jones, D.S., Fike, D.A., Eisenman, I., Hughes, N.C., Tripati, A.K., Fischer, W.W., 2011. The Magnitude and Duration of Late Ordovician–Early Silurian Glaciation. Science 331, 903–906.

Fiorella, R.P., Sheldon, N.D., 2017. Equable end Mesoproterozoic climate in the absence of high CO_2. Geology. doi:10.1130/G38682.1

Frantz, C.M., Petryshyn, V.A., Marenco, P.J., Tripati, A., Berelson, W.M., Corsetti, F.A., 2014.

Dramatic local environmental change during the Early Eocene Climatic Optimum detected using high resolution chemical analyses of Green River Formation stromatolites. Palaeogeogr. Palaeoclimatol. Palaeoecol. 405, 1–15.

Gallagher, T.M., Sheldon, N.D., Mauk, J.L., Petersen, S.V., Gueneli, N., Brocks, J.J., 2017. Constraining the thermal history of the North American Midcontinent Rift System using carbonate clumped isotopes and organic thermal maturity indices. Precambrian Res. 294, 53–66.

Geboy, N.J., Kaufman, A.J., Walker, R.J., Misi, A., de Oliviera, T.F., Miller, K.E., Azmy, K., Kendall, B., Poulton, S.W., 2013. Re–Os age constraints and new observations of Proterozoic glacial deposits in the Vazante Group, Brazil. Precambrian Res. 238, 199–213.

Ghosh, P., Adkins, J., Affek, H., Balta, B., Guo, W., Schauble, E.A., Schrag, D., Eiler, J.M., 2006. 13 C--18 O bonds in carbonate minerals: A new kind of paleothermometer. Geochim. Cosmochim. Acta 70, 1439–1456.

Gough, D.O., 1981. Solar interior structure and luminosity variations. Solar Phys. 74, 21–34.

Henkes, G.A., Passey, B.H., Grossman, E.L., Shenton, B.J., Pérez-Huerta, A., Yancey, T.E., 2014. Temperature limits for preservation of primary calcite clumped isotope paleotemperatures. Geochim. Cosmochim. Acta 139, 362–382.

Higgins, J.A., Blättler, C.L., Lundstrom, E.A., Santiago-Ramos, D.P., Akhtar, A.A., Crüger, Ahm AS, Bialik, O., Holmden, C., Bradbury, H., Murray, S.T., Swart, P.K. 2018. Mineralogy, early marine diagenesis, and the chemistry of shallow-water carbonates. Geochim. Cosmochim. Acta 220, 512-534.

Hren, M.T., Sheldon, N.D., 2012. Temporal variations in lake water temperature: Paleoenvironmental implications of lake carbonate $\delta^{18}O$ and temperature records. Earth Planet. Sci. Lett. 337–338, 77–84.

Hutchinson, D.R., White, R.S., Cannon, W.F., Schulz, K.J., 1990. Keweenaw hot spot: Geophysical evidence for a 1.1 Ga mantle plume beneath the Midcontinent Rift System. J. Geophys. Res. 95, 10869–10884.

Kah, L.C., Riding, R., 2007. Mesoproterozoic carbon dioxide levels inferred from calcified cyanobacteria. Geology 35, 799–802.

Kah, L.C., Sherman, A.G., Narbonne, G.M., Knoll, A.H., Kaufman, A.J., 1999. $\Delta^{13}C$ stratigraphy of the Proterozoic Bylot Supergroup, Baffin Island, Canada: implications for

797 regional lithostratigraphic correlations. Canadian Journal of Earth Sciences 36, 313–332.
798 Kasting, J.F., 1993. Earth's early atmosphere. Science 259, 920–926.
799 Kaufman, A.J., Xiao, S., 2003. High CO_2 levels in the Proterozoic atmosphere estimated from
800 analyses of individual microfossils. Nature 425, 279–282.
801 Laws, E.A., Popp, B.N., Bidigare, R.R., Kennicutt, M.C., Macko, S.A., 1995. Dependence of
802 phytoplankton carbon isotopic composition on growth rate and (CO2)aq: Theoretical
803 considerations and experimental results. Geochim. Cosmochim. Acta 59, 1131–1138.
804 Lepot, K., Benzerara, K., Rividi, N., Cotte, M., Brown, G.E., Philippot, P. 2009. Organic matter
805 heterogeneities in 2.72 Ga stromatolites: Alteration versus preservation by sulfur
806 incorporation. Geochim. Cosmochim. Acta 73, 6579-6599.
807 Lyons, T.W., Reinhard, C.T., Planavsky, N.J., 2014. The rise of oxygen in Earth's early ocean
808 and atmosphere. Nature 506, 307–315.
809 Mauk, J.L., Hieshima, G.B., 1992. Geochemistry of Metalliferous Black Shales Organic matter
810 and copper mineralization at White Pine, Michigan, U.S.A. Chem. Geol. 99, 189–211.
811 McCabe, B., 1985. The dynamics of 13C in several New Zealand lakes. University of Waikato.
812 McCollom, T.M., Seewald, J.S., 2006. Carbon isotope composition of organic compounds
813 produced by abiotic synthesis under hydrothermal conditions. Earth and Planetary Science
814 letters 243, 74–84.
815 Mitchell, R.L., Sheldon, N.D., 2016. Sedimentary provenance and weathering processes in the
816 1.1 Ga Midcontinental Rife of the Keweenaw Peninsula, Michigan, USA. Precambrian
817 Research 275, 225–240.
818 Mitchell, R.L., Sheldon, N.D., 2010. The ~1100 Ma Sturgeon Falls paleosol revisited:
819 implications for Mesoproterozoic weathering environments and atmospheric CO_2 levels.
820 Precam. Res. 183, 738–748.
821 Mitchell, R.L., Sheldon, N.D., 2009. Weathering and paleosol formation in the 1.1 Ga
822 Keweenawan Rift. Precambrian Research 168, 271–283.
823 Morey, G.B., Ojakangas, R.W., 1982. 7D: Keweenawan sedimentary rocks of eastern Minnesota
824 and northwestern Wisconsin. Geological Society of America Memoirs 156, 135–146.
825 Nishioka, G.K., Kelly, W.C., Douglas Elmore, R., 1984. Copper occurrences in stromatolites of
826 the Copper Harbor Conglomerate, Keweenaw Peninsula, northern Michigan. Econ. Geol.
827 79, 1393–1399.

828 Noffke, N., 2009. The criteria for the biogeneicity of microbially induced sedimentary structures
829 (MISS) in Archean and younger, sandy deposits. Earth-Sci. Rev. 96, 173–180.
830 Noffke, N., Awramik, S.M., 2013. Stromatolites and MISS—differences between relatives. GSA
831 Today 23, 4–9.
832 Ohr, M., 1993. Geochronology of diagenesis and low-grade metamorphism in pelites. University
833 of Michigan.
834 O'Leary, M.H., 1981. Carbon isotope fractionation in plants. Phytochemistry 20, 553–567.
835 Olson, S.L., Reinhard, C.T., Lyons, T.W., 2016. Limited role for methane in the mid-Proterozoic
836 greenhouse. Proc. Natl. Acad. Sci. U. S. A. 113, 11447–11452.
837 Pagès, A., Grice, K., Ertefai, T., Skrzypek, G., Jahnert, R., Greenwood, P., 2014. Organic
838 geochemical studies of modern microbial mats from Shark Bay: Part I: Influence of depth
839 and salinity on lipid biomarkers and their isotopic signatures. Geobiology 12, 469–487.
840 Parnell, J., Spinks, S., Andrews, S., Thayalan, W., Bowden, S., 2015. High Molybdenum
841 availability for evolution in a Mesoproterozoic lacustrine environment. Nat. Commun. 6,
842 6996.
843 Peters, K.E., Rohrback, B.G., Kaplan, I.R., 1981. Carbon and hydrogen stable isotope variations
844 in kerogen during laboratory-simulated thermal maturation. AAPG Bulletin 65, 501–508.
845 Peterson, S.V., Defliese, W.F., Saenger, C., Daëron, M., Huntington, K.W., John, C.M., Kelson,
846 J.R., Bernasconi, S.M., Coleman, A.S., Kluge, T., Olack, G.A., Schauer, A.J., Bjnai, D.,
847 Bonifacie, M., Breitenbach, S.F.M., Fiebig, J., Fernandez, A.B., Henkes, G.A., Hodell, .,
848 Katz, A., Kele, S., Lohmann, K.C., Passey, B.H., Peral, M.Y., Petrizzon, D.A., Rosenheim,
849 B.E., Tripati, A., Venturelli, R., Young, E.D., Winkelstern, I.Z. 2019. Effects of improved
850 17O correction on inter-laboratory agreement in clumped isotope calibrations, estimates of
851 mineral-specific offsets, and temperature dependence of acid digestion fractionation.
852 Geochem. Geophys. Geosys. Doi:10.1029/2018gc008127
853 Petryshyn, V.A., Corsetti, F.A., Frantz, C.M., Lund, S.P., Berelson, W.M., 2016. Magnetic
854 susceptibility as a biosignature in stromatolites. Earth Planet. Sci. Lett. 437, 66–75.
855 Petryshyn, V.A., Lim, D., Laval, B.L., Brady, A., Slater, G., Tripati, A.K., 2015. Reconstruction
856 of limnology and microbialite formation conditions from carbonate clumped isotope
857 thermometry. Geobiology 13, 53–67.
858 Planavsky, N.J., Cole, D.B., Isson, T.T., Reinhard, C.T., Crockford, P.W., Sheldon, N.D., Lyons,

T.W., 2018. A case for low atmospheric oxygen levels during Earth's middle history. Emerging Top. Life Sci., doi: 10.1042/ETLS20170161

Planavsky, N.J., Reinhard, C.T., Wang, X., Thomson, D., McGoldrick, P., Rainbird, R.H., Johnson, T., Fischer, W.W., Lyons, T.W., 2014. Earth history. Low mid-Proterozoic atmospheric oxygen levels and the delayed rise of animals. Science 346, 635–638.

Popp, B.N., Takigiku, R., Hayes, J.M., Louda, J.W., Baker, E.W., 1989. The post-Paleozoic chronology and mechanism of 13 C depletion in primary marine organic matter. Am. J. Sci. 289, 436–454.

Pratt, L.M., Summons, R.E., Hieshima, G.B., 1991. Sterane and triterpane biomarkers in the Precambrian Nonesuch Formation, North American Midcontinent Rift. Geochim. Cosmochim. Acta 55, 911–916.

Price, K.L., Huntoon, J.E., McDowell, D.S., 1996. Thermal history of the 1.1-Ga Nonesuch Formation, North American Mid-continent Rift, White Pine, Michigan. AAPG Bull. 80, 1–15.

Riding, R., 2011. The Nature of Stromatolites: 3,500 Million Years of History and a Century of Research, in: Advances in Stromatolite Geobiology, Lecture Notes in Earth Sciences. Springer Berlin Heidelberg, pp. 29–74.

Roberson, A.L., Roadt, J., Halevy, I., Kasting, J.F., 2011. Greenhouse warming by nitrous oxide and methane in the Proterozoic Eon. Geobiology 9, 313–320.

Saenger, C., Affek, H.P., Felis, T., Thiagarajan, N., Lough, J.M., Holcomb, M., 2012. Carbonate clumped isotope variability in shallow water corals: Temperature dependence and growth-related vital effects. Geochim. Cosmochim. Acta 99, 224–242.

Schoell, M., 1984. Recent advances in petroleum isotope geochemistry. Organic Geochemistry 6, 645–663.

Sheldon, N.D., 2013. Causes and consequences of low atmospheric pCO_2 in the late Mesoproterozoic. Chem. Geol. 362, 224–231.

Sheldon, N.D., 2012. Microbially Induced Sedimentary Structures in the ca. 1100 Ma Terrestrial Midcontinent Rift of North America, in: Microbial Mats in Silicilastic Depositional Systems Through Time. pp. 153–162.

Sheldon, N.D., 2006. Precambrian paleosols and atmospheric CO_2 levels. Precambrian Res. 147, 148–155.

Shenton, B.J., Grossman, E.L., Passey, B.H., Henkes, G.A., Becker, T.P., Laya, J.C., Perez-Huerta, A., Becker, S.P., Lawson, M., 2015. Clumped isotope thermometry in deeply buried sedimentary carbonates: The effects of bond reordering and recrystallization. Geol. Soc. Am. Bull. 127, 1036–1051.

Shields, G., Veizer, J., 2002. Precambrian marine carbonate isotope database: Version 1.1. Geochem.-Geophys.-Geosyst. 3, 1 of 12–12 of 12.

Stein, C.A., Kley, J., Stein, S., Hindle, D., Keller, G.R., 2015. North America's Midcontinent Rift: When rift met LIP. Geosphere 11, 1607–1616.

Stüeken , E E , Bellefroid , E , Prave , A R , Asael , D , Planavsky , N & Lyons , T 2017 , ' Not so non-marine? Revisiting the Stoer Group and the Mesoproterozoic biosphere ' Geochemical Perspectives Letters 3 , 221-229 . DOI: 10.7185/geochemlet.1725

Swart, P.K. 2008. Global synchronous changes in the carbon isotopic composition of carbonate sediments unrelated to changes in the global carbon cycle. Proc. Nat. Acad. Sci. 105, 13741-13745.

Swanson-Hysell, N.L., Maloof, A.C., Weiss, B.P., Evans, D.A.D., 2009. No asymmetry in geomagnetic reversals recorded by 1.1-billion-year-old Keweenawan basalts. Nat. Geosci. 2, 713–717.

Taran, Y.A., Kliger, G.A., Sevastianov, V.S., 2007. Carbon isotope effects in the open-system Fischer-Tropsch synthesis. Geochimica et Cosmochimica Acta 71, 4474–4487.

Tripati, A.K., Eagle, R.A., Thiagarajan, N., Gagnon, A.C., Bauch, H., Halloran, P.R., Eiler, J.M., 2010. 13C–18O isotope signatures and "clumped isotope" thermometry in foraminifera and coccoliths. Geochim. Cosmochim. Acta 74, 5697–5717.

Walter, M.R., Veevers, J.J., Calver, C.R., Gorjan, P., Hill, A.C., 2000/3. Dating the 840–544 Ma Neoproterozoic interval by isotopes of strontium, carbon, and sulfur in seawater, and some interpretative models. Precambrian Res. 100, 371–433.

Wellman, C.H., Strother, P.K., 2015. The terrestrial biota prior to the origin of land plants (embryophytes): a review of the evidence. Palaeontology 58, 601–627.

Wilmeth, D.T., Dornbos, S.Q., Isbell, J.L., Czaja, A.D., 2014. Putative domal microbial structure in fluvial siliciclastic facies of the Mesoproterozoic (1.09 Ga) Copper Harbor Conglomerate, Upper Peninsula of Michiga, USA. Geobiology 12, 99–108.

920 Zhao, M., Reinhard, C.T., Planavsky, N.J., 2017. Terrestrial methane fluxes and Proterozoic
921 climate. Geology 46, 139–142.

Table 1. Δ_{47} data for stromatolite growth bands and sparite crystals.

Sample	δ_{47}	$\delta^{13}C$	$\delta^{18}O_{Raw}$	Δ_{47}	HG Slope	Slope[1]	Intercept[2]	Δ_{47}	T ℃[3]	Mean T ℃	s.e.	T ℃[4]	Mean T ℃	s.e.
A	-8.99	-1.69	31.41	0.009	0.0254	1.0989	1.020	0.596	52			46		
A	-10.73	-1.65	30.13	0.009	0.0254	1.0989	1.020	0.616	47	50	2.7	40	43	2.6
A_2	-7.12	-2.54	31.93	0.040	0.0311	1.0611	0.923	0.754	16			11		
A_2	-5.73	-1.38	32.26	0.033	0.0311	1.0611	0.923	0.645	40	28	11.7	34	22	11.5
B	-7.40	-1.42	31.75	0.012	0.0254	1.0989	1.020	0.661	36			30		
B	-4.80	-1.13	32.45	0.012	0.0254	1.0989	1.020	0.648	39			33		
B	-3.52	-1.36	32.37	0.007	0.0254	1.0989	1.020	0.612	48	41	3.7	42	35	3.7
C	-7.85	-1.31	31.64	0.009	0.0254	1.0989	1.020	0.595	53			46		
C	-7.15	-1.13	31.81	0.006	0.0254	1.0989	1.020	0.588	54			48		
C	-6.66	-1.10	32.04	0.010	0.0254	1.0989	1.020	0.622	45	51	3.6	39	44	3.6
D	-8.72	-1.37	31.61	0.026	0.0269	1.0586	1.059	0.677	32			26		
D	-8.96	-1.37	31.56	0.025	0.0311	1.0611	0.923	0.615	47	40	7.4	41	34	7.3
A_sparite	-7.13	-1.63	31.14	0.013	0.0254	1.0989	1.020	0.608	49			43		
A_sparite	-7	-1.31	32.29	0.023	0.0311	1.0611	0.923	0.528	72	61	11.7	66	54	11.4
B_Sparite	-6.59	-1.33	32.27	0.021	0.0269	1.0586	1.059	0.654	38			31		
B_Sparite	-8.97	-1.25	31.87	0.025	0.0269	1.0586	1.059	0.623	45	41	3.8	39	35	3.7

[1] Transfer function slope

[2] Transfer function intercept

[3] Calculated temperature using Ghosh 2006 temperature equation adjusted to the ARF after Dennis et al. 2011

[4] Calculated temperature using Defliese et al. 2015

Table 2. Organic Carbon Data

Stromatolite	$\delta^{13}C$	Weight %
MI-UP-P	-24.0	0.140
MI-UP-Q	-25.5	0.043
MI-UP-S	-27.4	0.199
MI-UP-T	-26.3	0.106
Matrix Carbonate	$\delta^{13}C$	Weight %
MI-UP-O	-25.0	0.184
MI-UP-R	-26.0	0.219

			25 ℃	40 ℃	25℃	40 ℃	25 ℃	40 ℃
Sample (stromatolite)	$\delta^{13}C$	$\delta^{18}O$	Calculated $\delta^{13}C_{CO2aq}$[2]	Calculated $\delta^{13}C_{CO2aq}$[2]	ε_p[3]	ε_p[4]	ε_p[3]	ε_p[4]
CH-A	-1.4	23.2	-11.1	-9.9	16.7	15.1	18.0	16.3
CH-B	-1.2	23.9	-10.9	-9.7	17.0	15.3	18.2	16.5
CH-C	-1.2	23.9	-10.9	-9.7	16.9	15.3	18.2	16.5
CH-D	-1.2	23.8	-10.9	-9.7	16.9	15.3	18.2	16.5
CH-F	-1.2	23.7	-11.0	-9.8	16.9	15.2	18.1	16.5
CH-I	-0.9	23.7	-10.6	-9.4	17.2	15.6	18.5	16.8
CH-J	-0.9	23.7	-10.6	-9.4	17.3	15.6	18.5	16.9
CH-K	-0.8	23.9	-10.5	-9.3	17.4	15.7	18.6	17.0
CH-L	-0.8	24.1	-10.5	-9.3	17.3	15.7	18.6	16.9
CH-M	-0.9	23.7	-10.7	-9.5	17.2	15.5	18.4	16.8
Mean	**-1.1**	**23.8**	**-10.8**	**-9.6**	**17.1**	**15.4**	**18.3**	**16.7**
1 Δ_{47} Temperature ℃								
2 Calculated $\delta^{13}C_{CO2aq}$ using the temperature specified and the temperature dependent $\alpha_{calcite\text{-}CO2aq}$ of Deines et al. (1974)								
3 $\varepsilon_p = 1000*(\delta^{13}C_{CO2}-\delta^{13}C_p)/(1000+\delta^{13}C_p)$ after Laws et al. (1995) using the minimum $\delta^{13}C_{org}$ as δ_p.								
4 $\varepsilon_p = 1000*(\delta^{13}C_{CO2}-\delta^{13}C_p)/(1000+\delta^{13}C_p)$ after Laws et al. (1995) using the mean $\delta^{13}C_{org}$ as δ_p.								

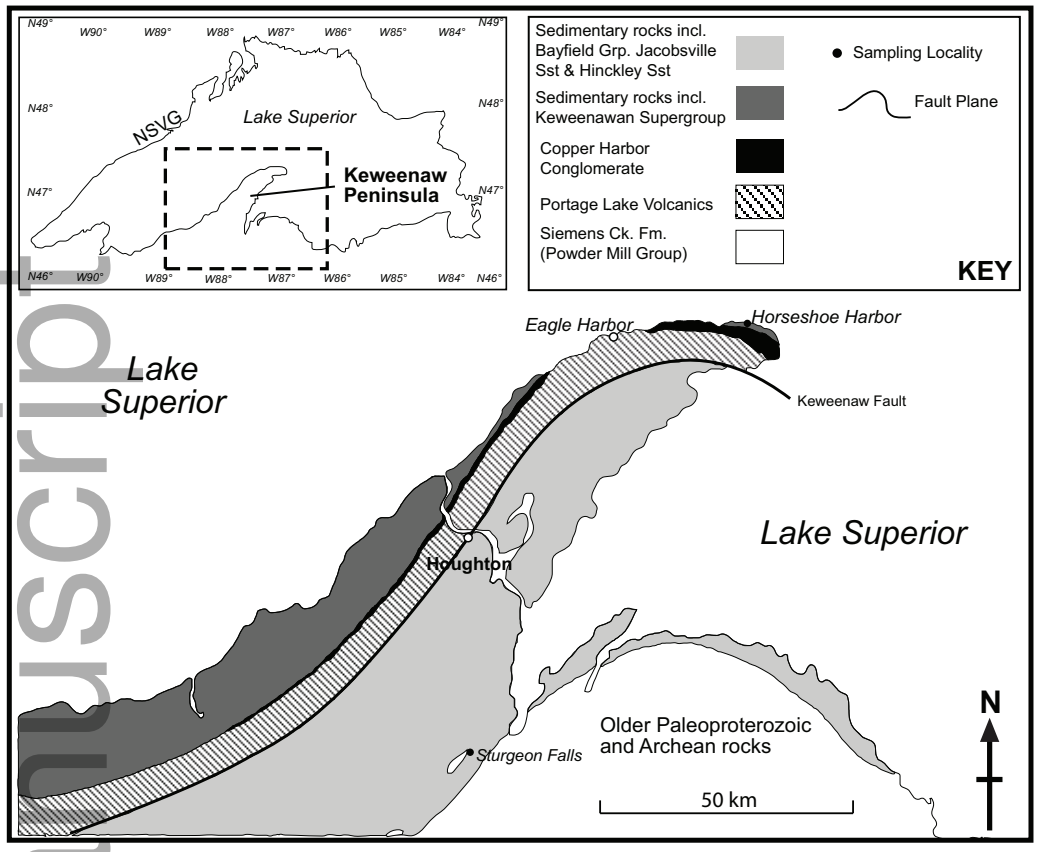

Figure 2.

dep2_79_f2.eps

Figure 3

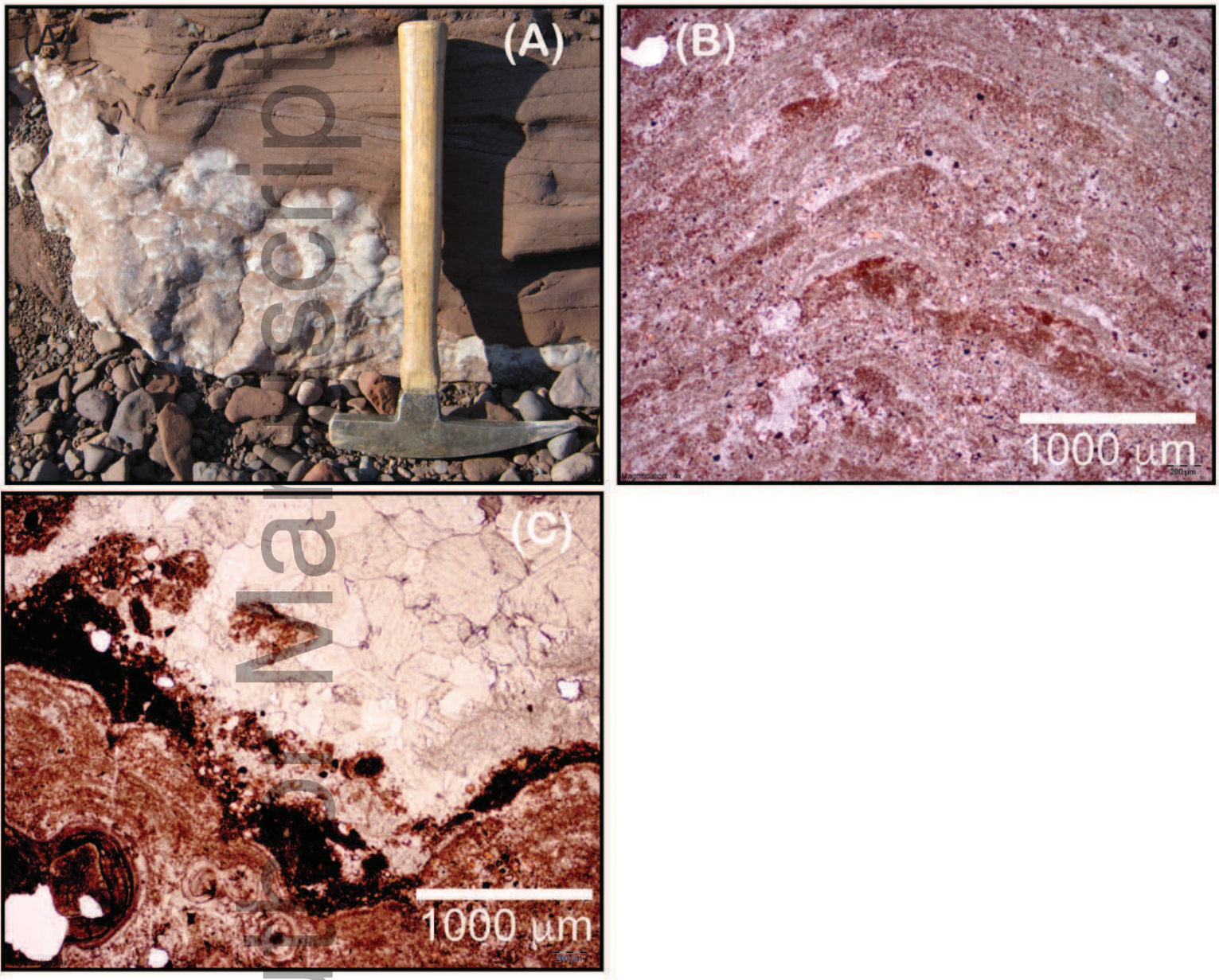

dep2_79_f3.eps

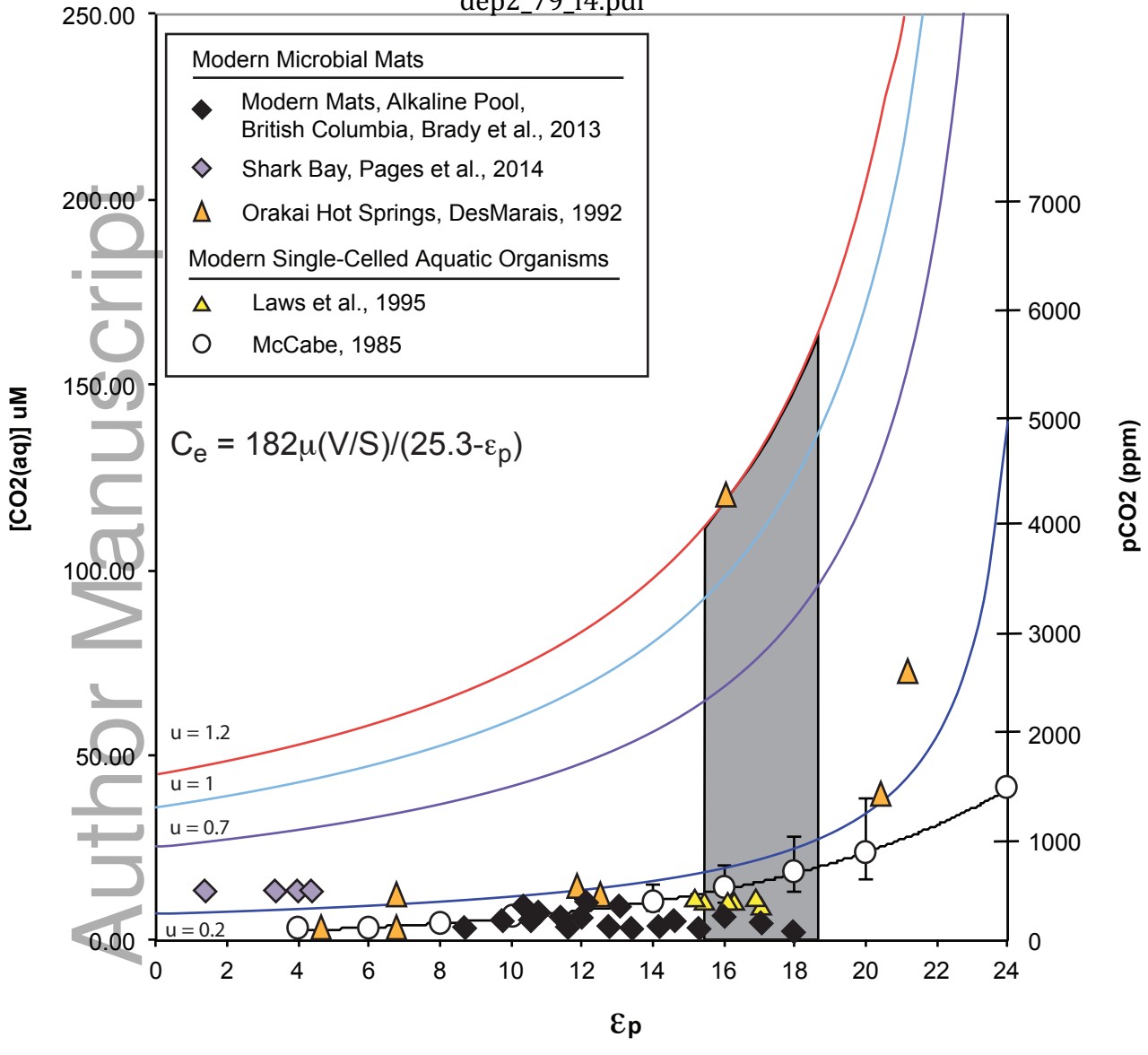

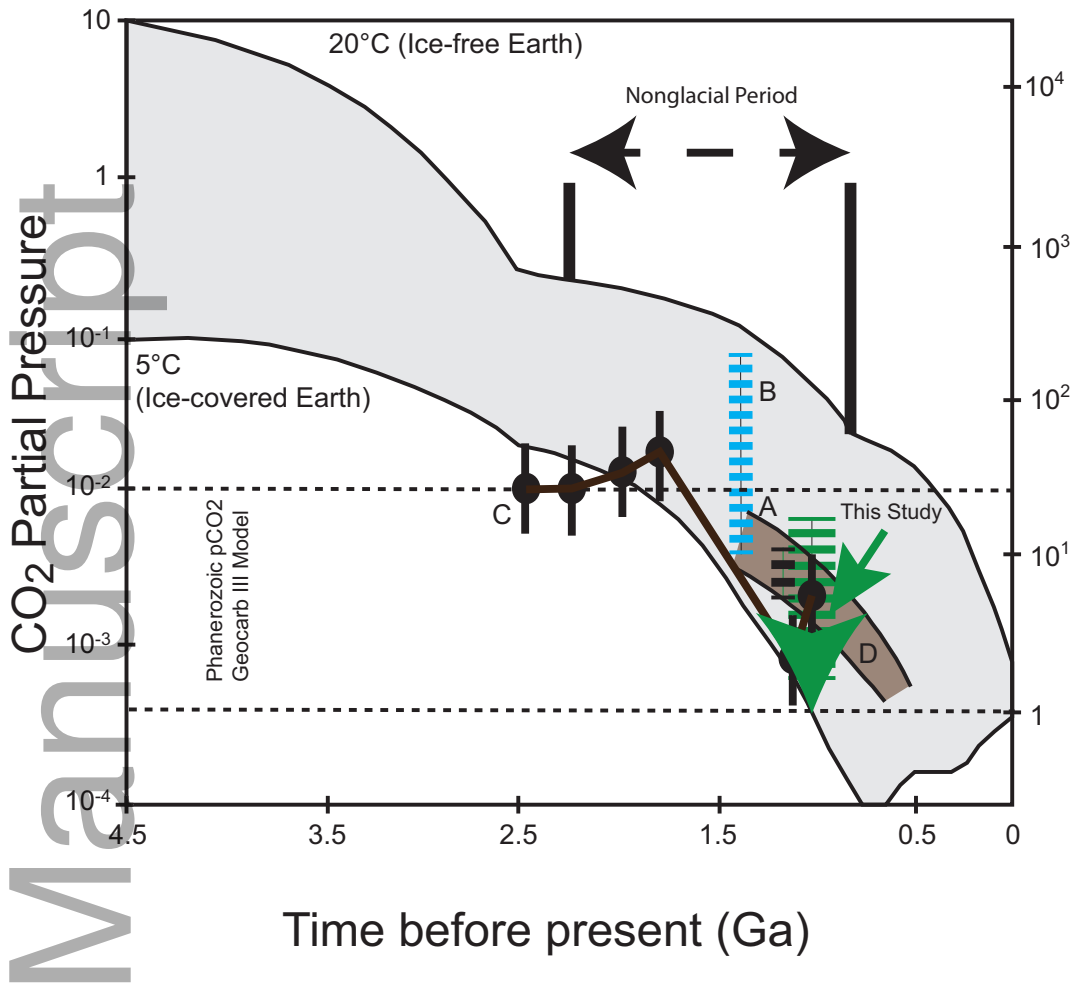

dep2_79_f5.eps